Electrocatalytic activity of Au nanoparticles onto TiO_2 nanotubular layers in oxygen electroreduction reaction: size and support effects

Hanna Maltanava[a], *Sergey Poznyak*[a,]*, *Maksim Starykevich*[b], *Maria Ivanovskaya* [a]

[a]Research Institute for Physical Chemical Problems, Belarusian State University, 220030 Minsk, Belarus

[b]Department of Materials and Ceramics Engineering, CICECO-Aveiro Institute of Materials, The University of Aveiro, 3810-193 Aveiro, Portugal

*Corresponding Author.

E-mail: poznyak@bsu.by

Author Contributions

The manuscript was written through contributions of all authors. All authors have given approval to the final version of the manuscript.

Abstract: Electrocatalytic activity of both bare high-ordered TiO_2 nanotubes (TNTs) and gold nanoparticles (Au NPs) loaded TNTs toward oxygen reduction reaction (ORR) has been examined by cyclic voltammetry (CV). Cyclic voltammograms for Au NPs-TNT electrodes are characterized by an additional wave observed at less negative potentials which is responsible for oxygen electroreduction on the surface of gold NPs. The overpotential for O_2 reduction on the Au surface grows with increasing the temperature of TNT annealing and the Au NPs size. The nature of the effects observed was explained by peculiarities of the electron transport through Schottky barrier formed at the Au NPs – TiO_2 interface. The width of the Schottky barrier, determined by semiconductor doping level and Au NPs size, plays a key role in the mechanism of electron transport through the space charge region.

Keywords: Electrocatalysis, Titanium dioxide, Nanotubes, Gold nanoparticles, Schottky barrier

1. Introduction

Oxygen reduction reaction (ORR) significantly limits widespread applications of fuel cells due to relatively slow kinetics of oxygen formation and decomposition on most electrodes [1]. Platinum and its alloys are mostly used as anode and cathode catalysts in these applications, but this metal is expensive and of limited reserve [2, 3]. Therefore, recently extensive research efforts have been devoted to the development of non-platinum electrocatalysts [4].Compared to the platinum-group metals, gold has attracted little attention in electrocatalysis, mainly because of its poor catalytic performance. However, bulk gold single crystal electrodes with (111), (110) and (100) orientation exhibit promising behavior in ORR. Thus, Au(100) electrode in alkaline medium displays the effectiveness in ORR close to

that of platinum [5]. In order to achieve a high specific surface area and particularly minimize the cost, gold is typically dispersed in the form of nanoparticles (NPs) and immobilized on solid surface [6, 7]. Although, amorphous carbon is considered to be the most used catalyst support for noble metal nanoparticles, its corrosion under cell operation media can lead to loss of electrocatalytical activity [8]. In searching for support materials, semiconductive oxides arouse considerable interest because of good physical-chemical properties and high stability in acid and alkaline solutions [9]. Besides, NPs of nobel metals supported by semiconductive oxides may enhance their catalytic activity owing to a strong metal support interaction (SMSI) effect, as reported for Pt/TiO_2 and Au/TiO_2 interfaces [10−13]. Nowadays, titania nanotubes (TNTs) become the object of a growing number of studies owing to the combination of unique properties such as huge surface area, low cost, high stability, nontoxicity and simple preparation procedure [14]. Recently, Macak et al. have reported the efficient oxygen electroreduction in acidic medium on layers of ordered TiO_2 nanotubes loaded with Au NPs [15].

The efficiency of metal-support systems in ORR can be strongly affected by both the metal-support interaction and the size and structure of metal NPs [16]. Guerin et al. demonstrated the specific activity of TiO_x-supported gold NPs with size ranging from 1.4 to 4.5 nm for oxygen reduction and concluded that the smaller particles require a large overpotential [17]. Tang et al. suggested a strong size effect of Au NPs, supported on carbon, and observed that the activity in ORR increased by 2.5 times for 3-nm gold NPs in comparison with that obtained with 7-nm NPs [18]. Also, Lee et al. investigated the activity of 3-, 6- and 8-nm carbon-supported Au NPs for ORR in alkaline medium and reported that the most effective were 8-nm particles [19]. More recently, Brülle et al. observed clear size-dependent ORR activity for Au NPs, deposited on HOPG and single-crystalline boron-doped diamond, in the range from 5 to 30 nm with a narrow size distribution, with increasing the

activity in ORR with a decrease in the NPs size [20]. However, Bron reported no size effect for Au NPs in the range between 2.7 and 42.3 nm supported on carbon black in acid solutions [21]. Thus, the literature data concerning the size effect of Au NPs on their electrocatalytic activity in ORR are contradictory and call for further investigation.

The main goal of the present research is to define the effect of TiO_2 semiconducting properties and gold NPs size on the efficiency of both bare TNT electrodes and Au NPs-loaded TNT ones in oxygen electroreduction reaction in an alkaline medium. We demonstrate a key role of the Schottky barrier formation at the Au NPs–TiO_2 interface on electron transport from the electrode bulk to the reactive species in solution.

2. Experimental

Titanium plates (4 cm × 1 cm; 99.7 % Ti, Alfa Aesar) were polished mechanically and then chemically in HF:HNO_3 (1:2 by volume) mixture to mirror finish and finally rinsed with deionized water. Self-organized highly ordered nanotubular titania layers were produced by two-steps anodization [22]. Electrolyte was 0.75% NH_4F and 2 vol. % H_2O in an ethylene glycol. The anodization procedure for both steps consisted of a potential ramp from 0 to 40 V (sweep rate - 200 mV s^{-1}) followed by holding the potential constant for 1 h. The oxide films formed during the first step of anodization were removed by detachment in an ultrasound bath with deionized water. Before the second anodization, the electrochemical cell was filled with a fresh portion of the electrolyte. After the second step of anodization, the samples were washed with ethanol and then their surface was cleaned from debris by treatment in an ultrasound bath with distilled water during 30 s. In order to obtain crystalline TiO_2 nanotubes, all samples were annealed at different temperatures ranging from 350 °C to 550 °C for 3 h in air.

To elucidate the effect of the Au NPs size on the catalytic activity of Au-TiO_2 electrodes in ORR, the Au NPs with different sizes were synthesized by the chemical reduction methods. Colloidal Au NPs with an average diameter of 5 nm were fabricated by $HAuCl_4$ reduction using sodium boron hydride as a reducing agent and sodium citrate as a stabilizer. First, 2mL of 5 mM $HAuCl_4$ aqueous solution was mixed with 2 mL of 10 mM Na_3Cit aqueous solution and diluted to 100 mL with DI water. Next, 270 μL of 0.5 M $NaBH_4$ solution was added dropwise to the resultant solution under vigorous stirring, giving rise to a red colored Au hydrosol. The synthesis was carried out at 18±2 °C.

Au NPs with a diameter of 15 and 25 nm were synthesized *via* a modified Frens method [23]. First, 100 mL of chloroauric acid with a final concentration of 0.3 and 0.6 mM, respectively, was transferred to a three-neck round bottom flask equipped with a stir bar and a condenser and placed in a hot oil bath. When the reflux started, calculated amount of 0.17 M sodium citrate solution was quickly poured to the flask to obtain the 10:1 molar ratio of citrate to gold(III) for 25-nm Au NPs and the 6:1 one for 15-nm Au NPs. Then, the reaction was allowed to run for 20 min, with the color of solution changing from yellow to ruby.

All solutions were prepared from reagent grade chemicals and deionized water.

The synthesized Au nanoparticles were deposited onto the TiO_2 nanotubes from colloidal solutions in an amount that allowed obtaining the same Au loading on the samples (3 μg/cm^2). After spreading the aqueous colloidal solution over the nanotubular oxide surface, the samples were vacuum-dried and then annealed at 200 °C for 1 h to eliminate water and to assure more intimate contact between the NPs and the TiO_2 surface.

The electrocatalytic activity of the TiO_2 and Au-TiO_2 electrodes in ORR was then examined by cyclic voltammetry (CV) using an Autolab PGSTAT 302N potentiostat in a 0.1 M KOH solution saturated with oxygen during 1 h. Electrochemical experiments were performed in a single-compartment glass cell using a standard three-electrode configuration.

An Hg/HgO electrode filled with 1 M KOH (Radiometer Analytical) and a Pt foil were used as the reference and counter electrodes, respectively. The potential sweep rate was 10 mV s^{-1}. Mott-Schottky measurements were performed while the dc polarization was applied by successive displacements of 50 or 100 mV in the cathodic direction from 0.6 V to –0.8 V with superimposing a sinusoidal perturbation (100 Hz with a modulation of 10 mV rms) onto dc bias voltage. At each sampled dc potential, the electrode was preconditioned for ~1 min before conducting the ac measurements. Before each experiment, oxygen was removed from the solution through Ar bubbling during 1 h.

The morphology of the samples and the Au particle size were studied using a Hitachi-4100 scanning electron microscope (SEM) and a LEO-640 transmission electron microscope (TEM). The composition of the Au-TNT layers was characterized by energy dispersive X-ray analyzer (EDX) fitted to the Hitachi-4100. X-ray diffraction measurements were carried out using a PANalytical Empyrean diffractometer (Cu K_α radiation). UV-Vis absorbance spectra of the gold sols were recorded using a Shimadzu UV-2550 spectrophotometer.

3. Results and discussion

3.1 Characterization of TiO_2 nanotubular layers and gold nanoparticles

Figure 1 shows typical SEM images of the TiO_2 nanotubular layers after their annealing. At the top of nanotubes, a relatively narrow distribution of the inner diameter (60±5 nm) and the wall thickness (12±2 nm) can be observed (Figure 1a). The cross-sectional view demonstrates well-aligned nanotubular arrays with a length of 10±1 μm (Figure 1b).

Figure 1

Figure 2a-c shows TEM images of the representatives of 5-, 15- and 25-nm Au NPs from the corresponding colloids. The resulting particles are nearly spherical and rather

uniform in size (Figure 2d-f). The surface plasmon resonance peak is observed in the UV-Vis spectra of the colloids (Figure 2g). The absorption peak slightly shifts from 514 to 525 nm with increasing the diameter of gold nanoparticles from 5 to 25 nm in good agreement with the literature data [24].

Figure 2

Figure 3a-c shows TEM and SEM images of the Au-loaded TiO_2 nanotubular layers. Gold nanoparticles can be found inside and on the surface of the TNT layers. The NPs are well separated and distributed inside nanotubes without aggregation. Energy dispersive X-ray analysis was used for determining the composition and revealed the presence of Au in the gold-modified TiO_2 nanotubular layers.

Figure 3

In order to evaluate the crystalline structure of the TiO_2 nanotubes as-prepared and annealed at different temperatures (350, 450 and 550 °C), XRD measurements were performed. The results obtained indicate that the as-prepared samples are amorphous and the annealed ones are polycrystalline. All annealed samples contain an anatase phase with (101), (103), (004), (112), (200), (105), (211) and (300) diffraction peaks at 25.3, 37.0, 37.9, 38.6, 48.1, 54.0, 55.1 and 82.3 °, respectively. The relative intensity of the (004) anatase peak is greater than that for standard TiO_2 anatase samples (JCPDS card No 84−1286). Rutile phase is present only in the TiO_2 sample annealed at 550 °C in a small amount.

3.2 Electrocatalytic activity of gold NPs/TiO_2 electrodes

The electrocatalytic activity of the Au NPs/TiO_2 electrodes in ORR was examined by cyclic voltammetry. Figure 4 displays cyclic voltammograms (CVs) of the TiO_2 nanotubular

electrode before (Figure 4a) and after (Figure 4b) deposition of 5-nm Au NPs. The recorded CV curves are for nine consecutive potential cycles in the oxygen saturated electrolyte. The voltammetric response of the bare TNT electrode shows two well defined waves at potentials more negative than –0.65 V. For the TNT electrode loaded with Au NPs, an additional wave, which can be related to oxygen electroreduction on the gold surface, appears at less negative potentials. It should be noted that there is an evolution of the CV curves during the cycling. The most pronounced difference is observed between the first and the subsequent scans, especially for Au-TiO_2 electrodes. The potential of the cathodic peak related to ORR on Au NPs shifts from –0.6 to –0.4 V during the cycling, while the position of the peaks at E < –0.65 V is not changed appreciably. Possible reasons of this effect will be discussed below. In order to compare CV curves for different electrodes in further consideration, we chose the cyclic voltammograms belonging to the ninth cycle (hereafter referred to as quasi-steady-state CVs), because after ninth cycle changing the CV curves mainly stopped.

Figure 4

Figure 5 presents quasi-steady-state cyclic voltammograms for bare TNT electrodes, annealed at different temperatures, in Ar-saturated (Figure 5a) and O_2-saturated (Figure 5b) 0.1M KOH solutions. The CVs recorded in Ar-saturated solutions are characterized by small cathodic peaks in the potential range from –0.2 to –0.7 V with broader anodic coupled peaks. Similar peaks were observed previously for both nanotubular TiO_2 layers and nanostructured titania thin films and attributed to filling/depopulation of deep trap states located at grain boundaries [25]. At potentials more negative than –0.8 V, a sharp rise of the cathodic current is observed in Ar-saturated solutions, and a significant anodic current is recorded during subsequent positive potential scan. This reversible electrochemical process can be assigned to

electron accumulation within the TiO_2 layer accompanied by charge compensation *via* proton uptake from electrolyte [26]:

$$Ti^{IV}O_2 + e^- + H^+ \leftrightarrow Ti^{III}O(OH) \quad (1)$$

As a result, electrochemical reductive doping of the titania electrode occurs.

In O_2-saturated solutions, oxygen reduction on the bare TNT electrodes is observed as an irreversible peak/wave at potentials more negative than –0.65 V. The limiting currents are quite similar for the TNT layers annealed at different temperatures, but half-wave potential for the TiO_2 annealed at 350 °C is shifted by 40 mV to more positive potentials; i.e., the overpotential for O_2 reduction grows slightly with increasing the temperature of TNT annealing. It is significant that the second cathodic peak at –0.9 V, which is observed for the bare TNT electrodes heated at 350 and 450 °C, practically disappears in the case of TNT electrode annealed at 550 °C (Figure 5b). Nature of this second peak still remains to be clarified. Mentus [27] suggested that oxygen reduction on TiO_2 electrodes proceeds through the interaction of O_2 molecules with Ti^{3+} ions generated at sufficiently high cathodic potentials. Baez et al. [28] proposed the mechanism of O_2 electroreduction involving electron-transfer mediation and assumed that surface-bound Ti^{IV}/Ti^{III} redox couple is the active catalytic agent. Taking into account the literature data [27, 28], the second peak may be tentatively attributed to acceleration of the O_2 electroreduction owing to additional Ti^{3+} generation occurring at $E < -0.8$ V according to the equation (1). Disappearance of this peak for the TNT electrode annealed at 550 °C can be explained by a significant decrease of the electrochemical doping rate for this electrode in comparison with those annealed at lower temperatures (Figure 5a).

Figure 5

Figure 6 shows quasi-steady-state CV curves recorded in O_2-saturated alkaline solutions at the TNT electrodes heated at different temperatures and loaded with 5-nm Au NPs. It is noteworthy that the position of the wave corresponding to ORR on Au NPs shifts significantly (by *ca.* 0.2V) to more negative potentials with increasing the temperature of TiO_2 support annealing from 350 to 550 °C.

Figure 6

This strong difference in the overvoltage for ORR, observed for the same Au NPs deposited on the TiO_2 crystalline nanotubular layers with the same nature but only annealed at different temperatures, can be rationalized by peculiarities of the electron transport through the Au/TiO_2 interface. In a point of the contact between Au nanoparticle and TiO_2 support, Schottky barrier is formed locally as a result of the equilibration of Fermi level in the metal and semiconductor (Figure 7a-c) [29−32]. Under cathodic polarization, electrons on the path from the TiO_2 bulk to Au NPs must penetrate through this barrier to participate further in the ORR on the Au surface (Figure 7b and 7c).

Figure 7

The efficiency and manner of the charge transfer *via* the metal–semiconductor interface depends mainly on the height (Φ_b) and the width (W_b) of the Schottky barrier (or space charge region - SCR) and can be realized by two major ways: thermionic emission and electron tunneling. When the W_b is large (in the case of weakly doped semiconductors), the probability of electron tunneling is insignificant and the predominant charge transfer mechanism is thermionic emission (Figure 7b). According to the thermionic emission theory, the electron flow depends strongly on the height of the potential barrier [33]. When the width of the SCR becomes narrower, the probability of electron tunneling increases sharply [34],

providing an additional way for electron transport through the Schottky barrier (Figure 7c). Generally, reduction of the W_b can be simply attained by increasing the density of electronic doping in a semiconductor [35]:

$$W_b = \left(\frac{2\varepsilon_0 \varepsilon \Phi_b}{eN_d}\right)^{1/2}, \quad (2)$$

where ε_0 is the vacuum permittivity, ε the relative permittivity, e the electron charge, N_d the ionized donor density, and Φ_b the height of the potential barrier.

In order to gain additional information about electronic properties of the TNT layers annealed at different temperatures, we performed capacitance measurements. Commonly the Mott-Schottky relation is used for characterization of the semiconductor/electrolyte interface [36]:

$$C_{SC}^{-2} = \left(\frac{2}{\varepsilon\varepsilon_0 e N_d S^2}\right)\left(E - E_{fb} - \frac{kT}{e}\right), \quad (3)$$

where C_{sc} is the differential capacitance of the space charge layer, S the surface of the semiconductor, E the applied potential, E_{fb} the flatband potential, k the Boltzmann's constant, and T the absolute temperature. Although the Mott-Schottky equation (3) was derived for single-crystal or polycrystalline compact electrodes, this analysis was also widely applied to nanostructured electrodes [37–41]. Strictly speaking, quantative determination of the donor concentration (N_d) for the TNT electrodes requires a complication of the Mott-Schottky model to take into account the tubular geometry of the TNT layers and their real surface area. However, in order to compare the doping level of the TNT layers annealed at different temperature but having similar geometry, here we used the simple equation (3) for estimation of apparent N_d values. In the capacitive region, the capacitance C_{sc} can be estimated from the equation [42]:

$$\mathrm{Im}(Z'') = (2\pi f C_{sc})^{-1}, \quad (4)$$

where Im(Z") is the imaginary component of the measured impedance and f the frequency of the applied *ac* signal.

The C_{sc}^{-2} *vs.* potential plots for the TNT electrodes annealed at different temperatures are reported in Figure 8.

Figure 8

From the slope of the linear part (at negative potentials) of the C_{sc}^{-2} *vs.* E plots and its intercept with the potential axis, the doping density and the flat band potential can be determined, respectively (Figure 8**)**. The variation of the slope of the C_{sc}^{-2} *vs.* E curves is observed at potentials more positive than -0.4 V, -0.45 V and -0.3 V for TNT electrodes heated at 550°C, 450°C and 350°C, respectively. Such bend of the Mott-Schottky plots is a common feature observed for anodic titania films, and it can result from different reasons discussed in detail in the literature [43–53].

Table 1 summarizes the apparent N_d values and the E_{fb} values for the TNT films annealed at different temperatures, which was calculated from the Mott-Schottky plots assuming $\varepsilon = 57$ (the average of frequently reported ε values for anodic oxide films on titanium [43, 44, 46, 54–57].

Table 1

As can be seen from Table 1, increasing the annealing temperature leads to a decrease in the apparent N_d values, which results in widening the space charge region in the TiO_2 according to eq. (2) and in changing the mechanism of electron transport through this region. As a result, the shift of the gold-catalized oxygen reduction wave to cathodic direction is observed (Figure 6).

Along with heat treatment, the doping level in the titania films can be also governed by cathodic polarization owing to the electrochemical reductive self-doping process (eq. (1)) [25, 58].The observed evolution of the CV curves under cycling to potentials more negative than –0.8 V (Figure 4b) can be mainly attributed to this phenomenon. This assumption is supported by the fact that such evolution of the CV curves is reversible. In fact, after keeping the electrode, preliminarily subjected to cycling between 0.10 and –1.13V, for 20-30 min at a potential of 0.6 V, the initial state (cyclic voltammogram corresponding to the first scan on fresh Au NPs-TNT electrode) is restored.

Along with the strong influence of the TiO_2 annealing temperature on the ORR overvoltage for Au NPs deposited on the TNT surface, we revealed that the ORR wave position is size-dependent, i.e. the behavior of oxygen reduction is greatly affected by the Au NPs size. As shown in Figure 9a, the ORR peak potential is shifted from –0.54 V to –0.40 V when decreasing the Au NPs size from 25 to 5 nm for the Au-TNT electrodes annealed at 350 °C. The similar trend is also observed for the Au-TNT electrodes annealed at 450 °C. However, the responses from 15-nm and 25-nm Au NPs are superimposed on the ORR wave from TiO_2, and their position cannot be determined unambiguously (Figure 9b). The observed size-dependent effect can be explained by the interfacial metal–oxide electron transport. According to the data reported in refs. [34, 59–63], for small diodes of nanometer-range size the Schottky barrier can be much narrower in comparison to large diodes. Moreover, along the edge of the Me–semiconductor contact the local electric field has been shown to be significantly enhanced, which decreases the depletion region width as compared to that in the center of the contact [34, 59]. For bigger NPs these edge effects are proportionally smaller. The resultant narrowing of the barrier gives rise to an enhanced contribution of tunneling to the electric transport through the barrier [34, 63]. Thus, the effectiveness of electron tunneling via the barrier developed at the Au NPs–TNT interface should depend strongly on

the Au NPs size, because the Schottky barrier is affected by this size. This effect can be responsible for the observed lowering of the ORR overvoltage for smaller Au NPs deposited on the TNT electrodes (Figure 9).

Figure 9

4. Conclusions

Oxygen electroreduction reaction in alkaline solutions has been studied at bare TNT electrodes and at Au NPs loaded TNT ones with different doping levels in TiO_2 and various Au NP sizes. The electroreduction of oxygen molecules on the TNT electrodes demonstrates two distinctive irreversible peaks. The nature of the second peak at more negative potentials is explained by acceleration of ORR owing to the formation of surface Ti^{3+}. Electrochemical behavior of the Au NPs-TNTs in ORR differs from bare TNTs by appearance of an additional wave at less negative potentials owing to oxygen reduction on the gold surface. The electrocatalytic activity of Au NPs-TNTs toward O_2 reduction is found to be dependent on the Au NPs size and TiO_2 support doping level. The overpotential of O_2 reduction on the surface of Au NPs with a definite size increases with increasing the annealing temperature of TiO_2 support. Moreover, when the Au NPs size reduces, provided that the annealing temperature of the TNTs is the same, the overpotential of ORR decreases. Such support- and size-dependent behavior of the Au NPs loaded TNT electrodes has been explained by the formation of Schottky barrier at the Au–TiO_2 interface. The height and width of the space charge region determine the efficiency and manner of charge transfer through the metal–semiconductor interface. Significant decrease in the density of ionized donors in the TNTs with increasing the annealing temperature has been proved by Mott-Schottky analysis. The narrowing of the Schottky barrier as a result of increasing the electronic doping density in

TiO_2 brings a significant contribution of electron tunneling for electron transport through the Schottky barrier. In turn, the Au NPs of varying scale show major changes in the effectiveness of electron tunneling if the TiO_2 doping level is similar.

Acknowledgment

We gratefully acknowledge the financial support of the European Commission (Project 645662 – SMARCOAT - H2020-MSCA-RISE-2014) for this research.

References

[1] K. Kinoshita, Electrochemical Oxygen Technology, John Wiley & Sons, Inc.: New York, 1992.

[2] U.A. Paulus, A. Wokaun, G.G. Scherer, T.J. Schmidt, V. Stamenkovic, V. Radmilovic, N.M. Markovic, P.N. Ross, Oxygen Reduction on Carbon-Supported Pt-Ni and Pt-Co Alloy Catalyst, J. Phys. Chem. B 106 (2002) 4181–4191. doi: 10.1021/jp013442l

[3] R. Adzic, Recent advances in the kinetics of oxygen reduction, in: J. Lipkowski, P.N. Ross (Eds.), Electrocatalysis, Wiley-VCH, New York, 1998; pp. 197–242.

[4] Electrocatalysis in Fuel Cells: A Non- and Low- Platinum Approach, M. Shao (Ed.), Springer-Verlag, London, 2013.

[5] R.R. Adžić, N.M. Marković, V.B. Vešović, Structural effect in electrocatalysis: oxygen reduction on the Au(100) single crystal electrode, J. Electroanal. Chem. 165 (1984) 105–120. doi:10.1016/S0022-0728(84)80090-X

[6] M. Valden, X. Lai, D.W. Goodman, Onset of Catalytic Activity of Gold Clusters on Titania with the Appearance of Nonmetallic Properties, Science 281 (1998) 1647-1650. doi: 10.1126/science.281.5383.1647

[7] N. Lopez, T.V.W. Janssens, B.S. Clausen, Y. Xu, M. Mavrikakis, T. Bligaard, J.K. Nørskov, On the origin of the catalytic activity of gold nanoparticles for low-temperature CO oxidation, J. Catal. 223 (2004) 232–235. doi:10.1016/j.jcat.2004.01.001

[8] O.J. Curnic, P.M. Mendes, B.G. Pollet, Enhanced durability of a Pt/C electrocatalyst derived from Nafion-stabilised colloidal platinum nanoparticles, Electrochem. Commun. 12 (2010) 1017–1020. doi:10.1016/j.elecom.2010.05.013

[9] S. Trasatti, Interfacial Electrochemistry of Conductive Oxides for Electrocatalysis, in: A. Wieckowski (Ed.), Interfacial Electrochemistry, Theory, Experiment and Applications, Marcel Dekker Inc., New York, 1999, pp. 769−793.

[10] M. Haruta, S. Tsubota, T. Kobayashi, H. Kageyama, M.J. Genet, B. Delmon, Low-Temperature Oxidation of CO over Gold Supported on TiO_2, α-Fe_2O_3 and Co_3O_4, J. Catal. 144 (1993) 175–192. doi:10.1006/jcat.1993.1322

[11] S. Tsubota, D.A.H. Cunningham, Y. Bando, M. Haruta, Preparation of nanometer gold strongly interacted with TiO_2 and the structure sensitivity in low-temperature oxidation of CO, Stud. Surf. Sci. Catal. 91 (1995) 227–235. doi:10.1016/S0167-2991(06)81759-3

[12] B.C. Beard, P.N. Ross, Characterization of a Titanium-Promoted Supported Platinum Electrocatalyst, J. Electrochem. Soc. 133 (1986) 1839–1845. doi: 10.1149/1.2109033

[13] S.G. Neophytides, S.H. Zafeiratos, M.M. Jaksic, Selective Interactive Grafting of Composite Bifunctional Electrocatalysts for Simultaneous Anodic Hydrogen and CO Oxidation: I. Concepts and Embodiment of Novel-Type Composite Catalyst, J. Electrochem. Soc. 150 (2003) E512−E526. doi: 10.1149/1.1606456

[14] P. Roy, S. Berger, P. Schmuki, TiO_2 Nanotubes: Synthesis and Applications, Angew. Chem. Int. Ed. 50 (2011) 2904–2939. doi: 10.1002/anie.201001374

[15] J.M. Macak, F. Schmidt-Stein, P. Schmuki, Efficient oxygen reduction on layers of ordered TiO_2 nanotubes loaded with Au nanoparticles, Electrochem. Commun. 9 (2007) 1783–1787. doi:10.1016/j.elecom.2007.04.002

[16] F.J. Vidal-Iglesias, J. Sola-Gullón, E. Herrero, J.M. Feliu, Au Electrocatalysis for Oxygen Reduction, in: M. Shao (Ed.), Electrocatalysis in Fuel Cells: A Non- and Low-Platinum Approach, Springer-Verlag, London, 2013, pp. 483−512.

[17] S. Guerin, B.E. Hayden, D. Pletcher, M.E. Rendall, J.-P. Suchsland, A Combinatorial Approach to the Study of Particle Size Effects on Supported Electrocatalysts: Oxygen Reduction on Gold, J. Comb. Chem. 8 (2006) 679−686. doi: 10.1021/cc060041c

[18] W. Tang, H. Lin, A. Kleiman-Shwarsctein, G. D. Stucky, E. W. McFarland, Size-Dependent Activity of Gold Nanoparticles for Oxygen Electroreduction in Alkaline Electrolyte, J. Phys. Chem. C 112 (2008) 10515−10519. doi: 10.1021/jp710929n

[19] Y. Lee, A. Loew, S. Sun, Surface- and Structure-Dependent Catalytic Activity of Au Nanoparticles for Oxygen Reduction Reaction, Chem Mater. 22 (2009) 755–761. doi: 10.1021/cm9013046

[20] T. Brülle, W. Ju, P. Niedermayr, A. Denisenko, O. Paschos, O. Schneider, U. Stimming, Size-dependent electrocatalytic activity of gold nanoparticles on HOPG and highly boron-doped diamond surfaces, Molecules 16 (2011) 10059–10077. doi: 10.3390/molecules161210059.

[21] M. Bron, Carbon black supported gold nanoparticles for oxygen electroreduction in acidic electrolyte solution, J. Electroanal Chem. 624 (2008) 64–68. doi:10.1016/j.jelechem.2008.07.026

[22] J.M. Macak, S.P. Albu, P. Schmuki, Towards ideal hexagonal self-ordering of TiO_2 nanotubes, Phys. Status Solidi RRL 1 (2007) 181–183. doi: 10.1002/pssr.200701148

[23] K. Zabetakis, W.E. Ghann, S. Kumar, M.-C. Daniel, Effect of high gold salt concentrations on the size and polydispersity of gold nanoparticles prepared by an extended Turkevich-Frens method, Gold Bull. 45 (2012) 203−211. doi:10.1007/s13404-012-0069-2

[24] M.-C. Daniel, D. Astruc, Gold Nanoparticles: Assembly, Supramolecular Chemistry, Quantum-Size-Related Properties, and Applications toward Biology, Catalysis, and Nanotechnology, Chem. Rev. 104 (2004) 293−346. doi: 10.1021/cr030698+

[25] T. Berger, T. Lana-Villarreal, D. Monllor-Satoca, R. Gómez, Charge transfer reductive doping of nanostructured TiO_2 thin films as a way to improve their photoelectrocatalytic performance, Electrochem. Commun. 8 (2006) 1713–1718. doi:10.1016/j.elecom.2006.08.006

[26] L.A. Lyon, J.T. Hupp, Energetics of the Nanocrystalline Titanium Dioxide/Aqueous Solution Interface: Approximate Conduction Band Edge Variations between H_0 = –10 and H_- = +26, J. Phys. Chem. B 103 (1999) 4623–4628. doi: 10.1021/jp9908404

[27] S.V. Mentus, Oxygen reduction on anodically formed titanium dioxide, Electrochim. Acta 50 (2004) 27–32. doi:10.1016/j.electacta.2004.07.009

[28] V. B. Baez, J. E. Graves, D. Pletcher, The reduction of oxygen on titanium oxide electrodes, J. Electroanal. Chem. 340 (1992) 273–286. doi:10.1016/0022-0728(92)80303-L

[29] A. Stevanovic, S. Ma, J. T. Yates Jr., Effect of Gold Nanoparticles on Photoexcited Charge Carriers in Powdered TiO_2−Long Range Quenching of Photoluminescence, J. Phys. Chem. C 118 (2014) 21275−21280. doi: 10.1021/jp507156p

[30] A. Vittadini, A. Selloni, Small gold clusters on stoichiometric and defected TiO_2 anatase (101) and their interaction with CO: A density functional study, J. Chem. Phys. 117 (2002) 353−361. doi: http://dx.doi.org/10.1063/1.1481376

[31] T. Minato, T. Susaki, S. Shiraki, H.S. Kato, M. Kawai, K.-i. Aika, Investigation of the electronic interaction between TiO_2(110) surfaces and Au clusters by PES and STM, Surf. Sci. 566−568 (2004) 1012−1017. doi:10.1016/j.susc.2004.06.047

[32] N. Kruse, S. Chenakin, XPS characterization of Au/TiO_2 catalysts: Binding energy assessment and irradiation effects, Appl. Catal. A 391 (2011) 367−376. doi:10.1016/j.apcata.2010.05.039

[33] S.M. Sze, Physics of Semiconductor Devices, John Wiley & Sons, Inc., New York, 1969, pp. 378−381.

[34] J. Hou, S.S. Nonnenmann, W. Qin, D.A. Bonnell, A transition in mechanisms of size dependent electrical transport at nanoscale metal-oxide interfaces, Appl. Phys. Lett. 103 (2013) 252106–252106-5. doi: http://dx.doi.org/10.1063/1.4851937

[35] W. Schottky, Zur Halbleitertheorie der Sperrschicht- und Spitzengleichrichter, Z. Phys. 113 (1939) 367−414. doi:10.1007/BF01340116

[36] P. Schmuki, H. Böhni, J.A. Bardwell, *In Situ* Characterization of Anodic Silicon Oxide Films by AC Impedance Measurements, J. Electrochem. Soc. 142 (1995) 1705–1712. doi: 10.1149/1.2048644

[37] A.G. Mũnoz, Semiconducting properties of self-organized TiO_2 nanotubes, Electrochim. Acta 52 (2007) 4167–4176. doi:10.1016/j.electacta.2006.11.035

[38] L.V. Taveira, A.A. Sagüés, J.M. Macak, P. Schmuki, Impedance Behavior of TiO_2 Nanotubes Formed by Anodization in NaF Electrolytes, J. Electrochem. Soc. 155, 2009, C293–C302. doi: 10.1149/1.2898503

[39] H. Tsuchiya, J.M. Macak, A. Ghicov, A.S. Räder, L. Taveira, P. Schmuki, Characterization of electronic properties of TiO_2 nanotube films, Corr. Sci. 49 (2007) 203–210. doi:10.1016/j.corsci.2006.05.009

[40] B.P. Nelson, R. Candal, R.M. Corn, M.A. Anderson, Control of Surface and ζ Potentials on Nanoporous TiO_2 Films by Potential-Determining and Specifically Adsorbed Ions, Langmuir 16 (2000) 6094–6101. doi: 10.1021/la9911584

[41] G.K. Boschloo, A. Goossens, J. Schoonman, Photoelectrochemical Study of Thin Anatase TiO_2 Films Prepared by Metallorganic Chemical Vapor Deposition, J. Electrochem. Soc. 144 (1997) 1311–1317. doi: 10.1149/1.1837590

[42] L.-k. Tsui, T. Homma, G. Zangari, Photocurrent Conversion in Anodized TiO_2 Nanotube Arrays: Effect of the Water Content in Anodizing Solutions, J. Phys. Chem. C 117 (2013) 6979–6989. doi: 10.1021/jp400318n

[43] S. Piazza, L. Calà, C. Sunseri, F. Di Quarto, Influence of the crystallization process on the photoelectrochemical behaviour of anodic TiO_2 films, Ber. Bunsenges. Phys. Chem. 101 (1997) 932–942. doi: 10.1002/bbpc.19971010608

[44] D.J. Blackwood, L.M. Peter, The influence of growth rate on the properties of anodic oxide films on titanium, Electrochim. Acta 34 (1989) 1505–1511. doi:10.1016/0013-4686(89)87033-1

[45] T. Ohtsuka, T. Otsuki, The influence of the growth rate on the semiconductive properties of titanium anodic oxide films, Corr. Sci. 40 (1998) 951–958. doi:10.1016/S0010-938X(98)00032-8

[46] M. Schneider, S. Schroth, J. Schilm, A. Michaelis, Micro-EIS of anodic thin oxide films on titanium for capacitor applications, Electrochim. Acta 54 (2009) 2663–2671. doi:10.1016/j.electacta.2008.11.003

[47] A.I. Sa, C.M. Rangel, P. Skeldon, G.E. Thompson, Semiconductive properties of anodic niobium oxides, Port. Electrochim. Acta 24 (2006) 305–311. ISSN 0872-1904.

[48] J.W. Schultze, U. Stimming, J. Weise, Capacity and Photocurrent Measurements at Passive Titanium Electrodes, Ber. Bunsenges. Phys. Chem. 86 (1982) 276–282. doi: 10.1002/bbpc.19820860404

[49] E.-J. Lee, S.-I. Pyun, Analysis of nonlinear Mott-Schottky plots obtained from anodically passivating amorphous and polycrystalline TiO_2 films, J. Appl. Electrochem. 22 (1992) 156–160. doi: 10.1007/BF01023817

[50] K.D. Allard, M. Ahrens, K.E. Heusler, Wachstum und Auflösung anodisch erzeugter Oxidschichten auf Titan, Werkstoff. Korros. 26 (1975) 694–699. doi: 10.1002/maco.19750260904

[51] D. Zane, F. Decker, G. Razzini, Characterization of electrodeposited TiO_2 films, Electrochim. Acta 38 (1993) 37–42. doi:10.1016/0013-4686(93)80007-M

[52] S.U.M. Khan, W. Schmickler, The capacity of thin passive films, J. Electroanal. Chem. 108 (1980) 329–334. doi:10.1016/S0022-0728(80)80341-X

[53] S.K. Poznyak, D.V. Talapin, A.I. Kulak, Electrochemical oxidation of titanium by pulsed discharge in electrolyte, J. Electroanal. Chem. 579 (2005) 299–310. doi:10.1016/j.jelechem.2005.03.002

[54] J. Marsh, D. Gorse, A photoelectrochemical and *ac* impedance study of anodic titanium oxide films, Electrochim. Acta 1998, 43, 659–670. doi:10.1016/S0013-4686(97)00210-7

[55] J.F. McAleer, L.M. Peter, Photocurrent spectroscopy of anodic oxide films on titanium, Faraday Discuss. 70 (1980) 67–80. doi: 10.1039/DC9807000067

[56] C. Fonseca, M.G. Ferreira, M.C. Belo, Modelling of the impedance behaviour of an amorphous semiconductor Schottky barrier in high depletion conditions. Application to the study of the titanium anodic oxide/electrolyte junction, Electrochim. Acta 39 (1994) 2197–2205. doi:10.1016/0013-4686(94)E0174-X

[57] T. Hurlen, S. Hornkjøl, Anodic growth of passive films on titanium, Electrochim. Acta 36 (1991) 189–195. doi:10.1016/0013-4686(91)85200-Q

[58] H. Zhou, Y. Zhang, Electrochemically Self-Doped TiO_2 Nanotube Arrays for Supercapacitors, J. Phys. Chem. C 118 (2014) 5626−5636. doi: 10.1021/jp4082883

[59] D.L. Carroll, M. Wagner, M. Rühle, D.A. Bonnell, Schottky-barrier formation at nanoscale metal-oxide interfaces, Phys. Rev. B 55 (1997) 9792−9799. doi: http://dx.doi.org/10.1103/PhysRevB.55.9792

[60] C. Häggluns, V.P. Zhdanov, Charge distribution on and near Schottky nanocontacts, Physica E 33 (2006) 296–302. doi:10.1016/j.physe.2006.03.152

[61] R. Hiesgen, D. Meissner, Nanoscale Photocurrent Variations at Metal-Modified Semiconductor Surfaces, J. Phys. Chem. B 102 (1998), 6549–6557. doi: 10.1021/jp9816420

[62] R. Kraya, L.Y. Kraya, D.A. Bonnell, Orientation Controlled Schottky Barrier Formation at Au Nanoparticle-$SrTiO_3$ Interfaces, Nano Lett. 10 (2010) 1224–1228. doi: 10.1021/nl903651p

[63] G.D.J. Smit, S. Rogge, T.M. Klapwijk, Scaling of nano-Schottky-diodes, Appl. Phys. Lett. 81 (2002) 3852–3854. doi: http://dx.doi.org/10.1063/1.1521251

Figure Captions

Figure 1. SEM images: a top view (a) and a cross section (b) of TiO_2 nanotubular layers obtained by anodization in ethylene glycol electrolyte at 40 V for 1 h.

Figure 2. TEM images of the synthesized 5-(a), 15-(b) and 25-nm (c) gold nanoparticles and UV-vis spectra of the corresponding Au hydrosols (d).

Figure 3. TEM (a) and SEM (b, c) images of TiO_2 nanotubular layers loaded with 5- (a), 15-(b) and 25-nm (c) Au NPs.

Figure 4. CV curves of ORR in oxygen saturated 0.1 M KOH solution on nanotubular TiO_2 layers, annealed at 350 °C, before (a) and after loading 5-nm Au NPs (b). Arrows indicate the direction of changing the CVs for nine consecutive cycles.

Figure 5. CV curves in Ar(a) and O_2(b) saturated 0.1 M KOH solutions on nanotubular TiO_2 layers annealed at different temperatures.

Figure 6. CV curves of ORR in 0.1 M KOH solution on nanotubular TiO_2 layers heated at different temperatures and then loaded by Au nanoparticles with a diameter of 5 nm.

Figure 7. Energy band diagrams for TiO_2 and Au NPs before contact (a) and after forming of contact (b, c). In case of weakly doped semiconductor characterizing broad SCL, the predominant charge transfer mechanism is thermionic emission (b). At the same time, for highly doped electrode the contribution of electron tunneling increases due to narrowing of the SCR width (c).

Figure 8. Mott-Schottky plots obtained for the TNT electrodes annealed at different temperatures.

Figure 9. CV curves of ORR in oxygen saturated 0.1 M KOH solution on nanotubular TiO_2 layers annealed at 350 ^{o}C(a) and 450 ^{o}C(b) and loaded by Au nanoparticles of different sizes.

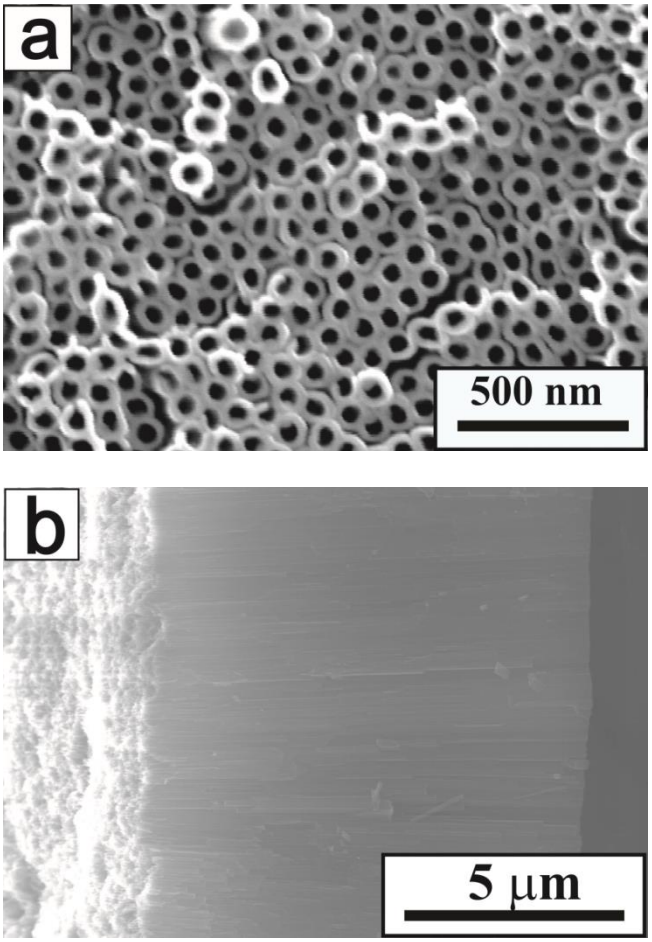

Figure 1.

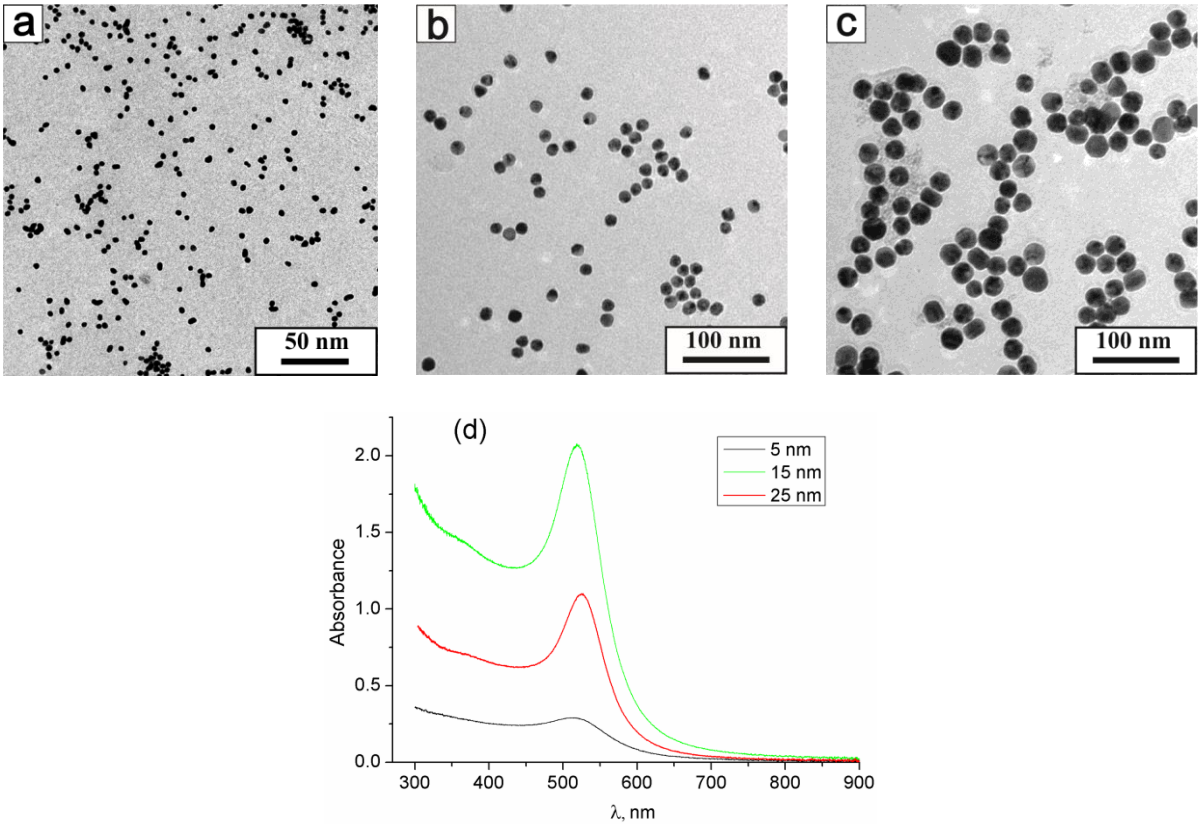
a
50 nm
b
100 nm
c
100 nm
(d)
5 nm
15 nm
25 nm
Absorbance
2.0
1.5
1.0
0.5
0.0
300
400
500
600
700
800
900
λ, nm

Figure 2.

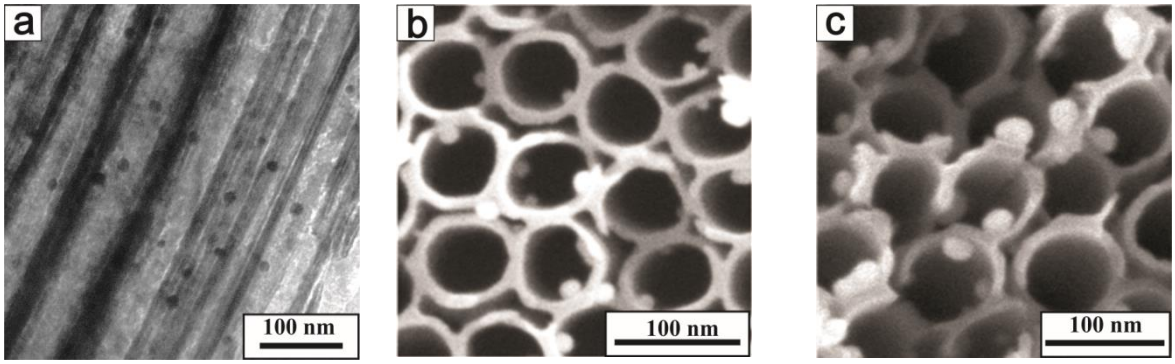

Figure 3.

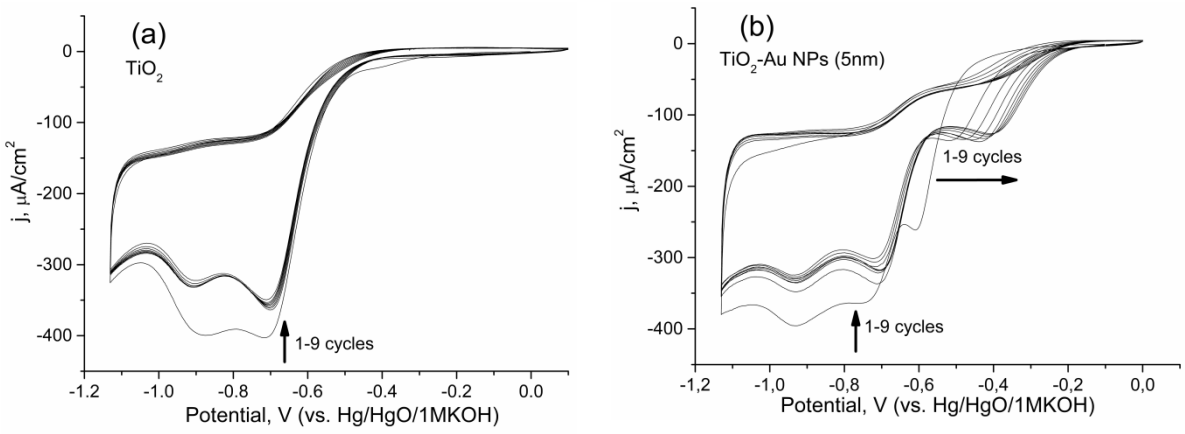
(a)
TiO2
0
-100
-200
-300
-400
j, μA/cm2
1-9 cycles
-1.2
-1.0
-0.8
-0.6
-0.4
-0.2
0.0
Potential, V (vs. Hg/HgO/1MKOH)
(b)
TiO2-Au NPs (5nm)
0
-100
-200
-300
-400
j, μA/cm2
1-9 cycles
1-9 cycles
-1,2
-1,0
-0,8
-0,6
-0,4
-0,2
0,0
Potential, V (vs. Hg/HgO/1MKOH)

Figure 4.

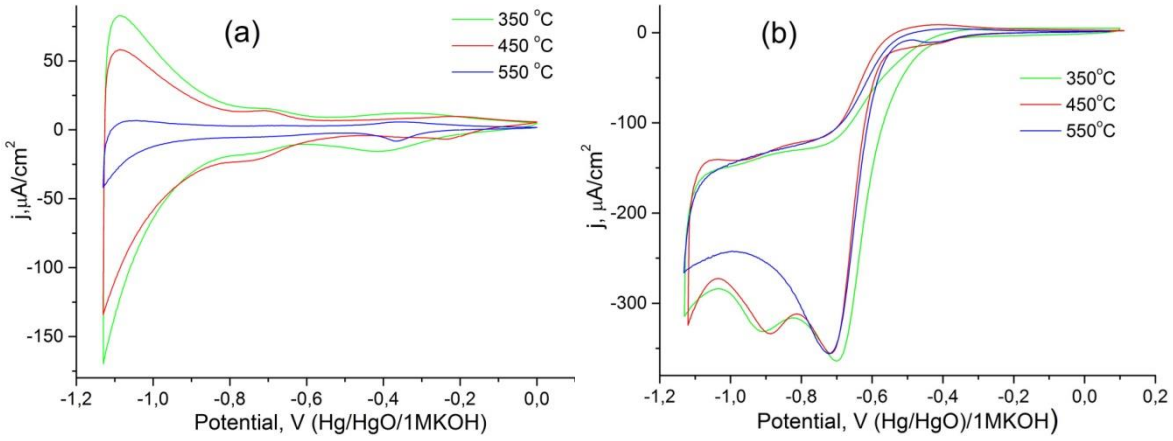
(a)
350 °C
450 °C
550 °C
j, μA/cm²
Potential, V (Hg/HgO/1MKOH)
(b)
350°C
450°C
550°C
j, μA/cm²
Potential, V (Hg/HgO)/1MKOH)

Figure 5.

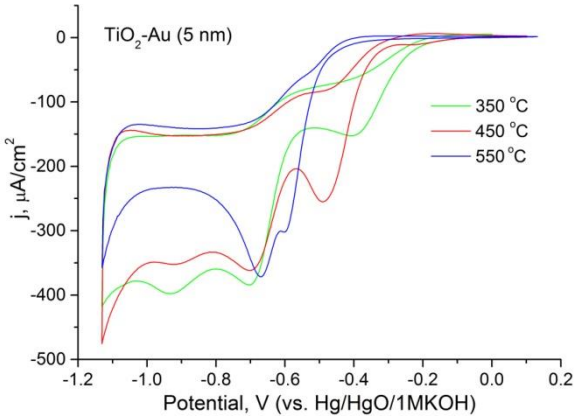
TiO2-Au (5 nm)
350 °C
450 °C
550 °C
j, μA/cm2
0
-100
-200
-300
-400
-500
-1.2
-1.0
-0.8
-0.6
-0.4
-0.2
0.0
0.2
Potential, V (vs. Hg/HgO/1MKOH)

Figure 6.

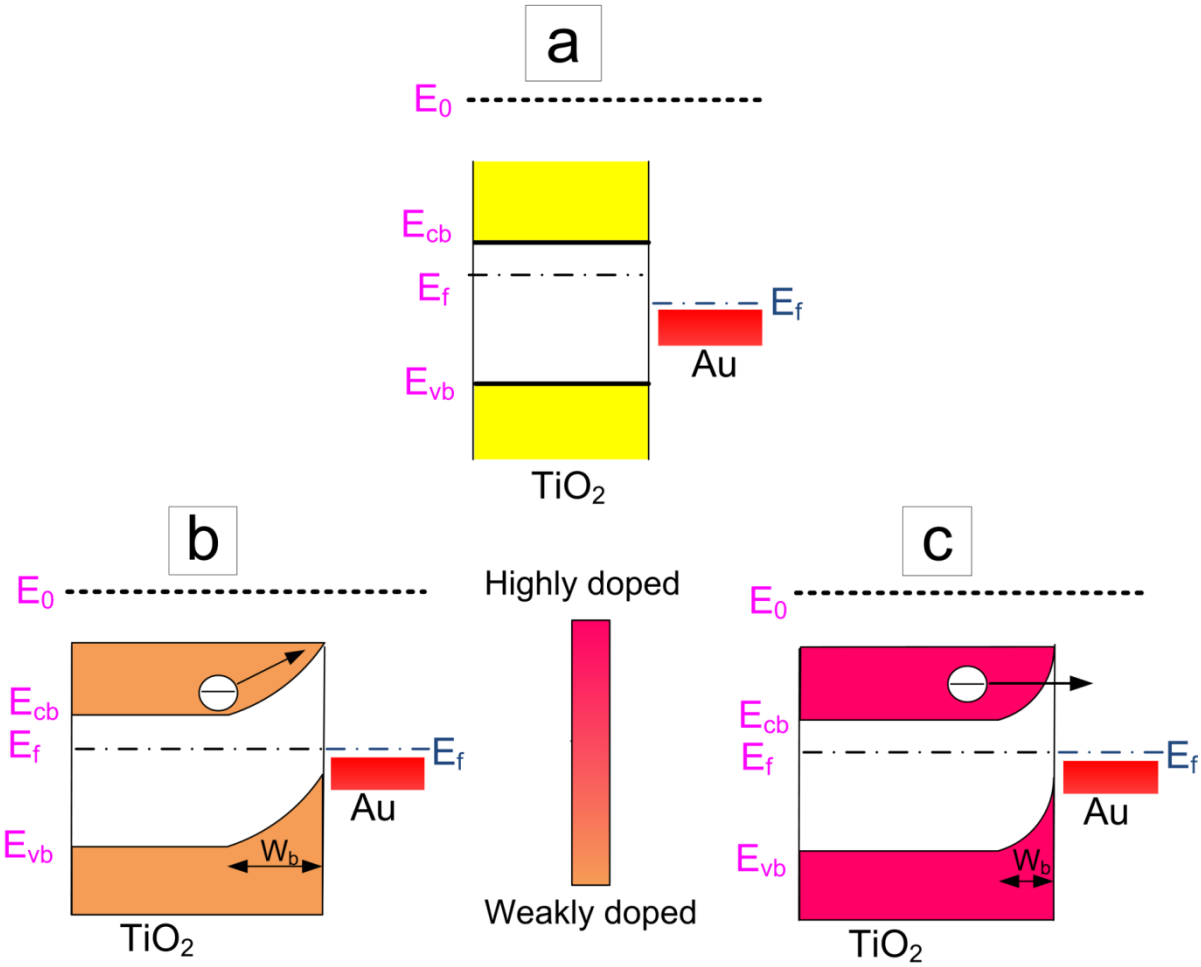
a
E0
Ecb
Ef
Evb
Ef
Au
TiO2
b
E0
Ecb
Ef
Evb
Ef
Au
Wb
TiO2
Highly doped
Weakly doped
c
E0
Ecb
Ef
Evb
Ef
Au
Wb
TiO2

Figure 7.

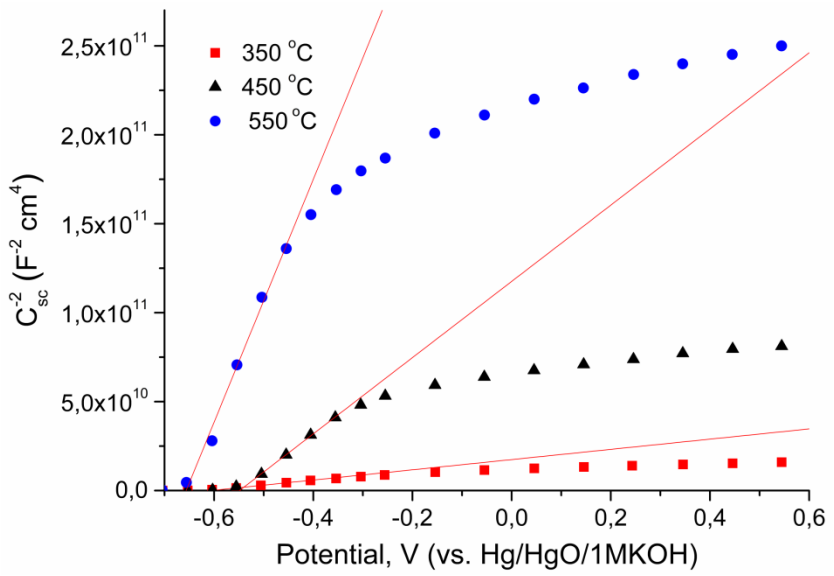
2,5x10^11
2,0x10^11
1,5x10^11
1,0x10^11
5,0x10^10
0,0
C^-2_sc (F^-2 cm^4)
350 °C
450 °C
550 °C
-0,6
-0,4
-0,2
0,0
0,2
0,4
0,6
Potential, V (vs. Hg/HgO/1MKOH)

Figure 8.

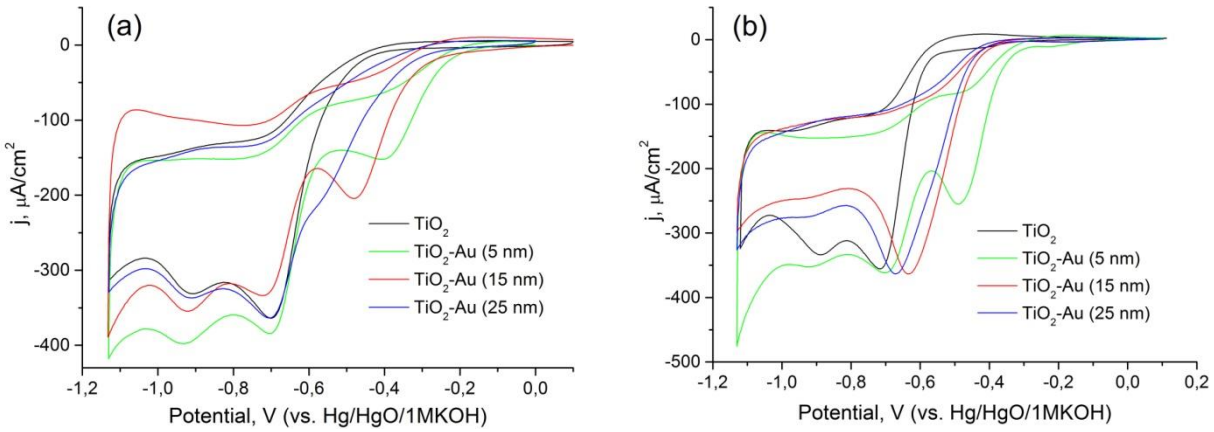
(a)
(b)
j, μA/cm2
Potential, V (vs. Hg/HgO/1MKOH)
TiO2
TiO2-Au (5 nm)
TiO2-Au (15 nm)
TiO2-Au (25 nm)

Figure 9.

Table 1. Semiconducting properties of the TNT electrodes annealed at different temperatures

Annealing temperature (^{o}C)	Apparent donor concentration (cm^{-3})	Flat band potential (V)
350	8.18×10^{19}	–0.61
450	1.10×10^{19}	–0.55
550	3.44×10^{18}	–0.65

Graphic abstract